



Transcriptomic analysis and laboratory experiments reveal potential critical genes and regulatory mechanisms in sepsis-associated acute kidney injury

Boyang Liu^{1#^}, Shengxiang Ao^{2#^}, Fang Tan^{1#}, Wei Ma², Haoru Liu², Huaping Liang², Xia Yang², Xinjin Chi¹

¹Department of Anesthesiology, The Seventh Affiliated Hospital of Sun Yat-sen University, Shenzhen, China; ²Department of Wound Infection and Drug, State Key Laboratory of Trauma, Burn and Combined Injury, Daping Hospital, Army Medical University (Third Military Medical University), Chongqing, China

Contributions: (I) Conception and design: X Chi, X Yang; (II) Administrative support: X Chi, X Yang; (III) Provision of study materials or patients: H Liang; (IV) Collection and assembly of data: B Liu, S Ao; (V) Data analysis and interpretation: B Liu, F Tan; (VI) Manuscript writing: All authors; (VII) Final approval of manuscript: All authors.

[#]These authors contributed equally to this work.

Correspondence to: Xinjin Chi, MD. Department of Anesthesiology, The Seventh Affiliated Hospital of Sun Yat-sen University, 628 Zhenyuan Street, Guangming District, Shenzhen 518107, China. Email: chixj@mail.sysu.edu.cn; Xia Yang, PhD. Department of Wound Infection and Drug, State Key Laboratory of Trauma, Burn and Combined Injury, Daping Hospital, Army Medical University (Third Military Medical University), 10 Changjiang Street, Yuzhong District, Chongqing 400042, China. Email: oceanyx@126.com.

Background: Sepsis-associated acute kidney injury (SA-AKI) is one of the most frequent and serious complications of sepsis. However, the transcriptional regulatory network of the pathophysiological mechanism of the kidney has not been revealed. This study identified new mechanisms in SA-AKI using bioinformatics analyses and laboratory-based experiments.

Methods: We performed transcriptomic profiling of mouse kidneys after cecal ligation and puncture (CLP) to mimic clinical sepsis. RNA from kidney samples from the CLP and control groups was isolated and analyzed using bulk messenger RNA (mRNA)-seq. Differentially expressed genes (DEGs) between the two groups were identified, and GO, KEGG and GSEA pathway enrichment analyses were performed. The protein-protein interaction (PPI) network of DEGs and hub genes was analyzed. The hub genes were verified using quantitative real-time polymerase chain reaction (qPCR) or Western blotting. The interaction network, targeted microRNAs (miRNAs) and long noncoding RNAs (lncRNAs) of hub genes were predicted, and the critical miRNA-hub gene regulatory axis was verified using qPCR, Western blotting, malondialdehyde (MDA) determination and flow cytometry. Correlation analyses of N6-adenosine methylation (m6A) RNA methylation regulators and hub genes and m6A modification analysis were performed.

Results: A total of 4,754 DEGs were identified between the two groups using high-throughput sequencing. The pathways in which DEGs were enriched included ferroptosis (the highest enrichment score), apoptosis, and the PI3K-Akt, NF-kappa B and IL-17 signaling pathways. Seven (*Hmox1*, *Spp1*, *Socs3*, *Mapk14*, *Lcn2*, *Cxcl1* and *Cxcl12*) of the 15 hub genes were involved in the KEGG pathway. mmu-miR-7212-5p-*Hmox1* was a key RNA regulatory axis in ferroptosis. m6A RNA methylation modifications were involved in SA-AKI. The correlation analyses showed the close interactions among the m6A RNA methylation regulators and important hub genes.

[^] ORCID: Boyang Liu, 0000-0002-6500-6505; Shengxiang Ao, 0000-0002-9284-3181.

Conclusions: The findings of this study provide new insights into the mechanism regulating the occurrence and progression of SA-AKI. The mmu-miR-7212-5p-Hmox1 axis in ferroptosis and m6A RNA methylation regulators may have potential clinical significance for the future treatment of SA-AKI. The datasets generated for this study can be found in the repository of the GEO database (Series number: GSE186822).

Keywords: Sepsis; acute kidney injury (AKI); bioinformatics analysis; ferroptosis; N6-adenosine methylation RNA methylation (m6A RNA methylation)

Submitted Feb 16, 2022. Accepted for publication May 24, 2022.

doi: 10.21037/atm-22-845

View this article at: <https://dx.doi.org/10.21037/atm-22-845>

Introduction

Sepsis is defined as a life-threatening organ dysfunction that results from the host's dysregulated response to infection (1). The kidney is one of the most common organs affected by sepsis, and it results in sepsis-associated acute kidney injury (SA-AKI), which poses a great challenge for clinicians (2,3). In critically ill patients with sepsis, acute kidney injury (AKI) is one of the most frequent and serious complications. It occurs in approximately 35–50% of patients with sepsis, and the mortality rate is as high as 35% (4,5). AKI increases the potential risk of chronic kidney disease, and surviving patients inevitably develop end-stage renal disease, which threatens the life and health of all humans (6,7). Therefore, it is vital to determine the pathophysiological mechanism of SA-AKI, and research on clinical therapeutic strategies for the treatment of SA-AKI is beneficial.

Transcriptomic sequencing analyses have been widely applied in a variety of diseases, including cancer, immune system diseases and infectious diseases, to seek novel pathways to improve diagnosis and treatment (8-10). Competitive endogenous RNA (ceRNA) networks are widely used to clarify new binding mechanisms between messenger RNAs (mRNAs), microRNAs (miRNAs), circular RNAs (circRNAs) and long noncoding RNAs (lncRNAs) to promote disease development at the transcriptome level (11,12). Bioinformatics analyses and related experimental verification using molecular biology analyses may help reveal potential key genes and critical pathways that contribute to the occurrence and progression of diseases (13). However, few studies focused on the bioinformatic analysis of SA-AKI. Tang (14) identified seven co-differentially expressed genes (DEGs) of septic shock and AKI, including *VMP1*, *SLPI*, *PTX3*, *TIMP1*, *OLFM4*, *LCN2* and *S100A9*, based on gene expression

datasets of the Gene Expression Omnibus (GEO), but their gene expression datasets were obtained from peripheral blood samples of humans, not directly from kidney samples of sepsis. Yang *et al.* (15) revealed the gene expression profile of SA-AKI by identifying prognosis-related genes, transcription factors, miRNAs and pathways. However, the hub genes among the DEGs were not identified using PPIs.

N6-adenosine methylation (m6A) is the most common posttranscriptional dynamic and reversible modification in eukaryotic mRNAs, and it constitutes approximately 0.4% of all adenosine nucleotides in RNAs (16). Three types of factors regulate m6A mRNA methylation: methyltransferases (writers, such as METTL3, METTL14 and WTAP), which install the methyl group on adenosine; demethylases (erasers, such as FTO and ALKBH5), which remove the methyl group; and binding proteins (readers, such as YTHDF, IGF2BPs and eIF3), which decode and interact with m6A modification (17).

m6A RNA methylation-related regulators influence mRNA fate decisions because they change local structure, affect the exportation of m6A-modified mRNA transcripts, facilitate mRNA translation and protein synthesis, and trigger the de-adenylation and degradation of transcripts (18). Moreover, m6A modifications are found in noncoding RNAs, such as lncRNAs, miRNAs and snRNAs, affect RNA-protein and RNA-RNA interactions or chromatin remodeling (19). lncRNAs also interact with m6A regulators to affect their function. It has been demonstrated that m6A RNA methylation plays important roles in a variety of biological processes, including cell differentiation, embryonic development, cell cycle regulation, circadian cycle, and stress responses (20,21). Growing evidence from *in vivo* and *in vitro* experiments and bioinformatic studies suggest that m6A RNA

methylation regulators are closely related to the occurrence, developmental pathogenesis, progression and clinical prognosis of various cancers and cardiovascular diseases (22,23). However, the role of m6A RNA methylation regulators in SA-AKI and their associations with SA-AKI genes were rarely studied.

The current study sequenced the RNAs of kidneys from a sepsis model group and control group mice, identified the DEGs and hub genes, and constructed co-expression and ceRNA networks. We verified the predicted results using laboratory-based experiments. We studied and validated key m6A RNA methylation regulators in sepsis and revealed a significant correlation between m6A RNA methylation regulators and DEGs. This study provides a novel perspective and lays the foundation to clarify the underlying pathophysiological mechanisms of SA-AKI. We present the following article in accordance with the ARRIVE reporting checklist (available at <https://atm.amegroups.com/article/view/10.21037/atm-22-845/rc>).

Methods

Animals and groups

C57BL/6 mice (male, 6–8 weeks old) were purchased from Guangdong Yaokang Biotechnology Co., Ltd. (China). We housed all mice in a standard environment, with a 12-h/12-h light-dark cycle, and the mice were free to eat and drink. According to a common sepsis protocol, we used the cecal ligation and puncture (CLP) method to construct a model of sepsis (24,25). For RNA sequencing, 5 mice were randomly divided into 2 groups: the CLP group (n=3) and the sham group (n=2). We anesthetized mice in the CLP group with 2–4% isoflurane. Under aseptic conditions, a 2-cm midline laparotomy was created below the diaphragm to expose the cecum. Two-thirds of the cecum was ligated with a 5-0 silk suture and punctured twice using a 22-gauge needle. The cecum was gently squeezed to extrude a small amount of feces through the perforation site. Animals were resuscitated with 1 mL of subcutaneous saline after CLP. The procedures of the sham group (controls) were the same as the CLP group, except for the ligation and perforation. The mice were sacrificed via neck fracture 6 hours after CLP, and the kidneys were taken for subsequent RNA sequencing. Six to eight weeks mice were used for quantitative real-time polymerase chain reaction (qPCR) (3 mice per group) and Western blotting (3 mice per group) verification, as described above, and the

only difference was that the kidneys for Western blotting analysis were taken 24 hours after CLP/sham surgery. To minimize variability across experiments, the same researcher performed all of the CLP/sham surgeries, and the other researchers who collected specimens and performed the subsequent experiments and data analyses were blinded to the group allocation. Experiments were performed under a project license (No. AMUWEC20201509) granted by the Laboratory Animal Welfare and Ethics Committee of Third Military Medical University, in compliance with the Third Military Medical University institutional guidelines for the care and use of animals.

RNA isolation and library preparation

Total RNA from kidney samples [CLP group (n=3) and sham group (n=2)] was extracted using TRIzol (Thermo Scientific, USA) reagent according to the manufacturer's protocol. RNA purity and quantification were evaluated using a NanoDrop 2000 spectrophotometer (Thermo Scientific, USA). RNA integrity was assessed using an Agilent 2100 Bioanalyzer (Agilent Technologies, Santa Clara, CA, USA). A total of 1 µg of RNA per sample was used as initial material for the RNA sample preparations. Ribosomal RNA was removed using a Ribo-off™ rRNA Depletion Kit (Human/Mouse/Rat) (Vazyme, China). The sequencing libraries were generated following the manufacturer's recommendations with varied index labels using the NEBNext® Ultra™ Directional RNA Library Prep Kit for Illumina (NEB, USA).

RNA sequencing and differentially expressed gene analysis

The libraries were sequenced on an Illumina NovaSeq 6000 platform, and 150-bp paired-end reads were generated. Raw data (raw reads) in FASTQ format were processed using fastp (version 0.20.0) (26) software with default parameters in paired end mode. Clean data were obtained for downstream analyses by removing reads containing adapters, reads containing poly-N and low-quality reads from the raw data. The clean reads were mapped to references (GRCm38) of mouse mRNAs and lncRNAs using bowtie2 (version 2.3.1) (27) with the parameters -k30 -t -p20. FPKM values and read counts of each transcript were obtained by eXpress (version 1.5.1) with the parameters—no-update-check—rf-stranded. Differential expression analysis was performed using the DESeq R package (27). The functions estimateSizeFactors

and `nbinomTest` were used to normalize the data and to calculate differential P values, respectively. A P value <0.05 and $\log_2(\text{fold change}) >1$ or <-1 were set as the thresholds for significantly differential expression. Hierarchical cluster analysis of DEGs was performed to explore gene expression patterns.

Heatmap and volcano plot analyses

To better visualize these DEGs, the R packages `heatmap` and `ggplot2` were used to draw heatmaps and volcano plots (28).

Enrichment analysis

Gene Ontology (GO) and Kyoto Encyclopedia of Genes and Genomes (KEGG) pathway enrichment analyses of DEGs were performed using R based on the hypergeometric distribution. To determine whether a gene set correlated with some phenotypic class distinction and assess the distribution trend of the genes of a predefined set, gene set enrichment analysis (GSEA) (29) software was used to analyze the gene expression profile at an overall level, and C5 (ontology gene sets) was chosen for functional enrichment analyses.

Construction of the PPI network

The protein-protein interaction (PPI) network was constructed based on DEGs using the online tool STRING (v11.5) (30). Considering the large number of DEGs, we further restricted the number of significant DEGs using stricter filter conditions: adjusted P value <0.01 and $\log_2\text{FoldChange} >3$ or <-3 . Ultimately, 814 DEGs were included to construct the PPI network.

For better analysis and visualization, we downloaded the interaction data and optimized the PPI network using Cytoscape software (v3.8.2). The Minimal Common Oncology Data Elements (MCODE) plugin was used to identify significant gene clusters (parameter: Degree Cutoff =2; Node Score Cutoff =0.2; K-Core =2; Max. Depth =100). The CytoHubba plugin was used to identify hub genes in the significant gene clusters. We used two different algorithms, degree and maximal clique centrality (MCC), to calculate the top 30 hub genes. All of the results of MCODE and CytoHubba (degree and MCC) were intersected to obtain the final hub genes.

Prediction of target miRNAs

We used three online miRNA databases [TargetScan (31), miRWalk (32), miRDB (33)] to predict the target miRNAs of hub genes involved in KEGG pathways. The target miRNAs were selected by taking the intersections of the 3 databases. The mRNA-miRNA co-expression network was constructed using Cytoscape software (v3.8.2).

Construction of the ceRNA network

Predicted target lncRNAs were obtained from the DIANA tools (LncBase Predicted v.2), LNCediting (34) and lncRNASNP2 databases, and the first three predicted lncRNAs of each database were selected based on the score. A ceRNA network was constructed based on the interactions among mRNAs, miRNAs, and lncRNAs using Cytoscape software (v3.8.2).

Correlation analysis of m6A RNA methylation-related regulators and hub genes

We selected 26 m6A RNA methylation-related regulators based on published reviews (35,36), and we restricted the regulators to 23 genes that were detected in these high-throughput sequencing data.

The PPI network of 23 m6A RNA methylation-related regulators was analyzed using STRING (v11.5) (30). The correlation of m6A RNA methylation-related regulators and hub genes was analyzed using the “Corrplot” package of R software (confidence level =0.95).

The m6A modifications analysis

The m6A modification sites were obtained from the RMBase (v2.0) database (37), which was based on the reanalysis of m6A-seq and methylated RNA immunoprecipitation sequencing (MeRIP-Seq) raw data.

Cell culture

Mouse kidney tubular epithelium cells (TCMK-1) were obtained from BeNa Culture Collection (Henan, China). The cells were maintained in a cell incubator at 37 °C in a 5% CO₂ humidified atmosphere in DMEM/F12 medium (Gibco; Thermo Fisher Scientific, Inc., MA, USA) supplemented with 10% fetal bovine serum (Gibco; Thermo Fisher

Scientific, Inc., CA, USA) and 1% penicillin/streptomycin.

Cell treatments and transfection

TCMK-1 cells were stimulated with lipopolysaccharide (LPS, L2630, Sigma-Aldrich, Darmstadt, Germany) to mimic sepsis *in vitro*. The mimics and inhibitors of miR-7212-5p were synthesized by RiboBio (Guangzhou, China). The cells were divided into six groups: (I) control; (II) miR-7212-5p mimic; (III) miR-7212-5p inhibitor; (IV) Control + LPS; (V) miR-7212-5p mimic + LPS; and (VI) miR-7212-5p inhibitor + LPS. Before transfection, TCMK-1 cells were plated in a 6-well plate at 1×10^6 cells/well, antibiotic-free medium was added, and the cells were 50–60% confluent after 24 h. The cell culture medium was changed to serum-free DMEM/F12 medium to prepare for transfection. The transfection process was performed according to the instructions of the riboFECTTMCP Transfection Kit (RiboBio, China). The cells in the miR-7212-5p mimic and miR-7212-5p mimic + LPS groups were transfected with 50 nM of a miR-7212-5p mimic using a riboFECTTMCP Transfection Kit and cultured for 48 h. The cells in the miR-7212-5p inhibitor and miR-7212-5p inhibitor + LPS groups were transfected with 100 nM of miR-7212-5p inhibitor using a riboFECTTMCP Transfection Kit and cultured for 48 h, following the manufacturer's instructions. After transfection for 48 h, the cells in the Control + LPS, miR-7212-5p mimic + LPS and miR-7212-5p inhibitor + LPS groups were stimulated with 100 $\mu\text{g}/\text{mL}$ LPS for 6 h (qPCR) or 24 h (Western blotting).

RNA extraction and qPCR

Total RNA was extracted from the kidney specimens, and the cells were collected using TRIzol reagent (Thermo Fisher Scientific, USA) following the manufacturer's instructions. The purity and quality of the total RNA were determined using a Nano Drop 1000 spectrophotometer (Thermo Fisher Scientific, USA). Briefly, 1,000 ng RNA derived from kidney tissues or TCMK-1 cells was reverse transcribed into cDNA using a PrimeScript TM RT reagent Kit (Takara, Japan) according to the manufacturer's protocol. The qRT-PCR was performed using the CFX96 real-time PCR system (Bio-Rad, CA, USA) with SYBR Premix Ex Taq TM II (Takara, Japan). Glyceraldehyde 3-phosphate dehydrogenase (GAPDH) served as an internal control for real-time PCR. PCR primers were designed and synthesized by Tsingke Biological Technology (Beijing, China). The relative expression of the genes in each experimental group was analyzed using the

$2^{-\Delta\Delta C_t}$ method. The sequences of the primers used in the qPCR experiments are listed in *Table 1*. All experiments were performed in triplicate.

Western blotting analysis

Frozen kidney tissue specimens from 6 mice (3 CLP mice, 3 sham mice) were weighed and cut into small pieces. Kidney single-cell suspensions were obtained by grinding followed by filtration through a 70- μm cell strainer. The pellets were treated with red blood cell lysis buffer (Beyotime Biotechnology Co., Ltd., Jiangsu, China) and washed twice with phosphate-buffered saline (PBS, HyClone Laboratories Inc., UT, USA) to remove red blood cells. The kidney tissue pellets or the TCMK-1 cell samples were added to protein lysis buffer with protease inhibitors. The samples were centrifuged at 12,000 $\times g$ for 30 minutes at 4 °C, and the supernatant was collected. The protein concentrations were measured using a BCA Protein Assay Kit (Beyotime Biotechnology Co., Ltd., Jiangsu, China). Equal amounts of total protein were separated using 10% Tris-Glycine extended stain-free polyacrylamide gels (Bio-Rad, CA, USA), and the proteins were transferred to polyvinylidene difluoride (PVDF) membranes (Roche, USA) using a wet blotting apparatus (Bio-Rad, CA, USA). The cells were blocked with 5% fat-free milk for 2 h at room temperature. The membranes were incubated with the following primary antibodies overnight at 4 °C: anti-METTL3 antibody (1:2,000, Arigobio, ARG56406), anti-ACSL4 (1:20,000, Abcam, ab155282), anti-ALKBH5 antibody (1:2,000, Abcam, ab69325), and anti-Hmox1 (1:1,000, Proteintech, 10701-1-AP). The cells were incubated with secondary antibodies (anti-rabbit IgG, 1:3,000, Cell Signaling Technology, 7074S; goat anti-mouse IgG, 1:10,000, ZSGB-BIO, 117228) at room temperature for 1 h. The blots were washed with TBST and visualized by enhanced chemiluminescence using a luminescent imaging workstation. The amount of protein was proportional to the optical density (OD) intensity, which was measured using ImageJ software (National Institutes of Health, MD, USA). Total protein was measured using a ChemiDoc Touch Imaging System (Bio-Rad, CA, USA) and used as a loading control. All the reactions were repeated 3 times.

ROS assay

TCMK-1 cells were divided into six groups: (I) Control; (II) miR-NC; (III) miR-7212-5p inhibitor; (IV) Control +

Table 1 Primers Sequences for qPCR and oligonucleotides sequences for miRNA mimic or inhibitor

Resource	Gene	Sequence (5'→3')	
Mouse	<i>Gaphd</i>	Forward	TGGAAAGCTGTGGCGTGAT
		Reverse	TGCTTCACCACCTTCTTGAT
Mouse	<i>Hmox1</i>	Forward	CGCCTTCCTGCTCAACAT
		Reverse	ACGAAGTGACGCCATCTG
Mouse	<i>Socs3</i>	Forward	TGCGCCTCAAGACCTTCAG
		Reverse	GCTCCAGTAGAATCCGCTCTC
Mouse	<i>Cxcl12</i>	Forward	GCTCTGCATCAGTGACGGTA
		Reverse	TAATTTCCGGTCAATGCACA
Mouse	<i>Cxcl1</i>	Forward	ACCGAAGTCATAGCCACACTC
		Reverse	CTCCGTTACTTGGGGACACC
Mouse	<i>Mapk14</i>	Forward	GGACTGTGAGCTGAAGATCCTA
		Reverse	CGCATCCAATTCAAGATGACCT
Mouse	<i>Spp1</i>	Forward	AAGAGCGGTGAGTCTAAGGAGTCC
		Reverse	TGGCTGCCCTTTCCGTTGTTG
Mouse	<i>Lcn2</i>	Forward	ACCACGGACTACAACCAGTTCCGCC
		Reverse	ACTTGCCAAAGCGGGTGAAACG
Mouse	<i>Acs14</i>	Forward	CTCACCATTATATTGCTGCCTGT
		Reverse	TCTCTTTGCCATAGCGTTTTTCT
Mouse	<i>iNOS</i>	Forward	TTGACGCTCGGAACTGTA
		Reverse	ACCTGATGTTGCCATTGTT
Mouse	<i>IL-6</i>	Forward	TAGTCCTTCCACCCCAATTTCC
		Reverse	TTGGTCCTTAGCCACTCCTTC

Table 1 (continued)**Table 1** (continued)

Resource	Gene	Sequence (5'→3')	
Mouse	<i>mmu-miR-7212-5p mimic</i>	Sense	UCUGGGGGCUUGUGUGGUAGG
		Antisense	CCUACCACACAAGCCCCCAGA
Mouse	<i>mmu-miR-7212-5p inhibitor</i>	Sense	CCUACCACACAAGCCCCCAGA
		Antisense	CCUACCACACAAGCCCCCAGA
Mouse	<i>mmu-miR-NC</i>	Sense	CAGUACUUUUGUGUAGUACAAA

qPCR, quantitative real-time polymerase chain reaction; miRNA, microRNA.

LPS; (V) miR-NC + LPS; and (VI) miR-7212-5p inhibitor + LPS. After transfection for 48 h, the cells in the Control + LPS, miR-NC + LPS and miR-7212-5p inhibitor + LPS groups were stimulated with 100 µg/mL LPS for 24 h. Intracellular ROS levels were estimated using flow cytometry and an ROS assay kit (S0033S, Beyotime Biotechnology Co., Ltd., Jiangsu, China) according to the manufacturer's protocol. Briefly, TCMK-1 cells were incubated with the fluorescent probe DCFH-DA. The cells were analyzed using flow cytometry with an excitation wavelength of 488 nm and an emission wavelength of 525 nm. The ROS levels were measured using the mean fluorescence intensity with FlowJo software (version 10.7, BD Biosciences, NJ, USA).

Determination of malondialdehyde (MDA) level

Grouping and treatment were the same as the ROS assay. The level of MDA was determined using a colorimetric method and an MDA content assay kit (Solarbio Life Sciences, BC0025, Beijing, China) according to the manufacturer's instructions.

Statistical analysis

SPSS 25.0 software (IBM Corp., Armonk, NY, USA) was used for statistical analyses. Normally distributed variables were assessed using Student's *t*-test to compare

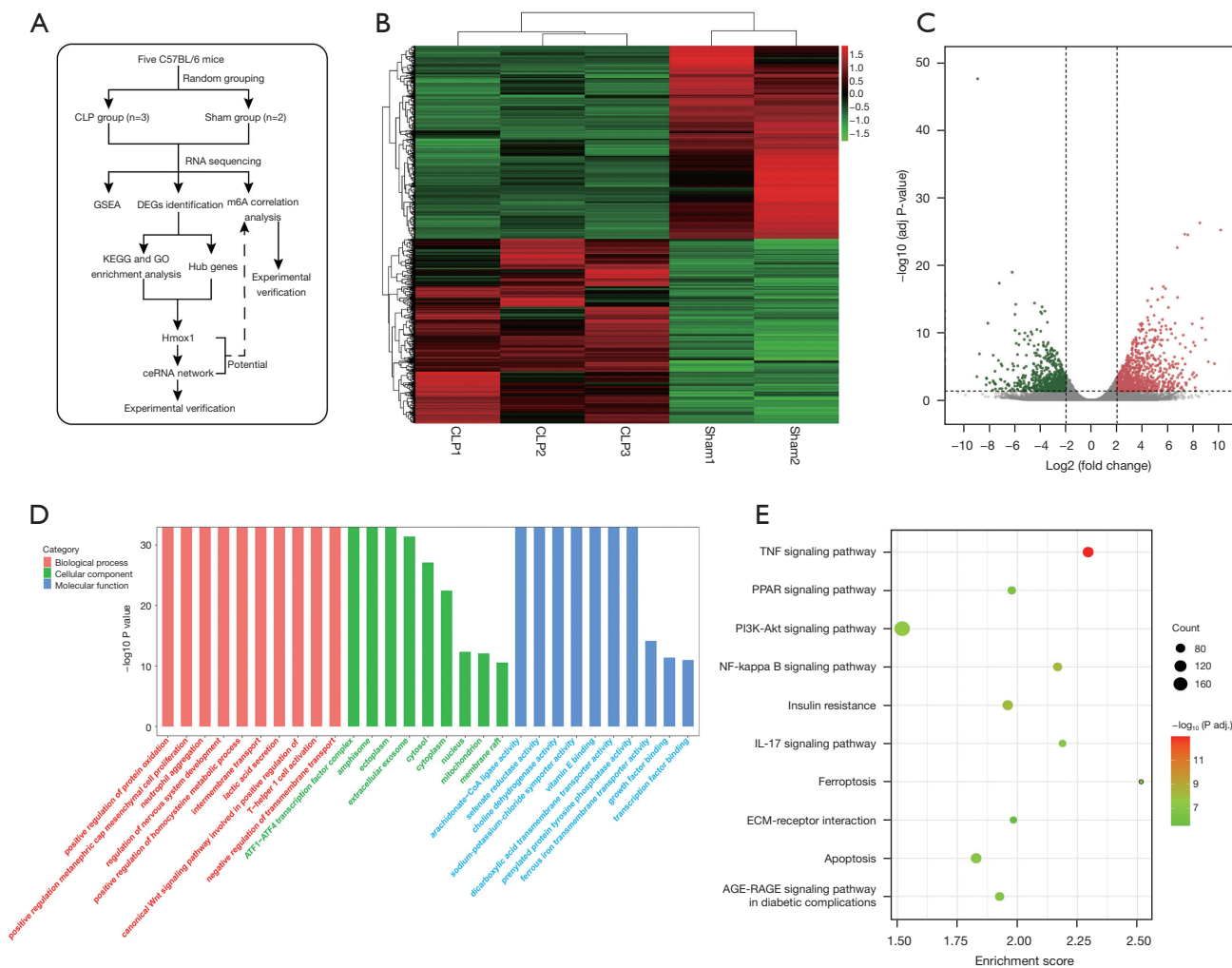


Figure 1 Identification of DEGs for enrichment analysis. (A) Experimental flow chart. (B) Heatmap of DEGs between the CLP and sham samples. Red areas represent high expression, and green areas represent low expression. (C) Volcano plot of DEGs between the CLP and sham samples. The red plots represent upregulated genes, the green plots represent downregulated genes, and the gray plots represent nonsignificant genes. (D) GO pathway enrichment analyses of DEGs. The bar graph shows the top 10 (red for biological processes and blue for molecular function) and the top 9 (green for cellular component) enriched GO pathways. (E) KEGG pathway enrichment analyses of DEGs. The bubble plot shows the most enriched KEGG pathways. The closer the color of a dot is to red, the smaller its P value is, and the closer the color is to green, the larger the P value is. CLP, cecal ligation and puncture; GSEA, gene set enrichment analysis; DEGs, differentially expressed genes; m6A, N6-adenosine methylation; KEGG, Kyoto Encyclopedia of Genes and Genomes; GO, Gene Ontology.

the differences between the two groups, and nonnormally distributed variables were detected using the nonparametric Mann-Whitney U test. Statistical significance was set at a P value of <0.05.

Results

Identification of DEGs for enrichment analysis

As shown in the experimental flow chart (Figure 1A), five

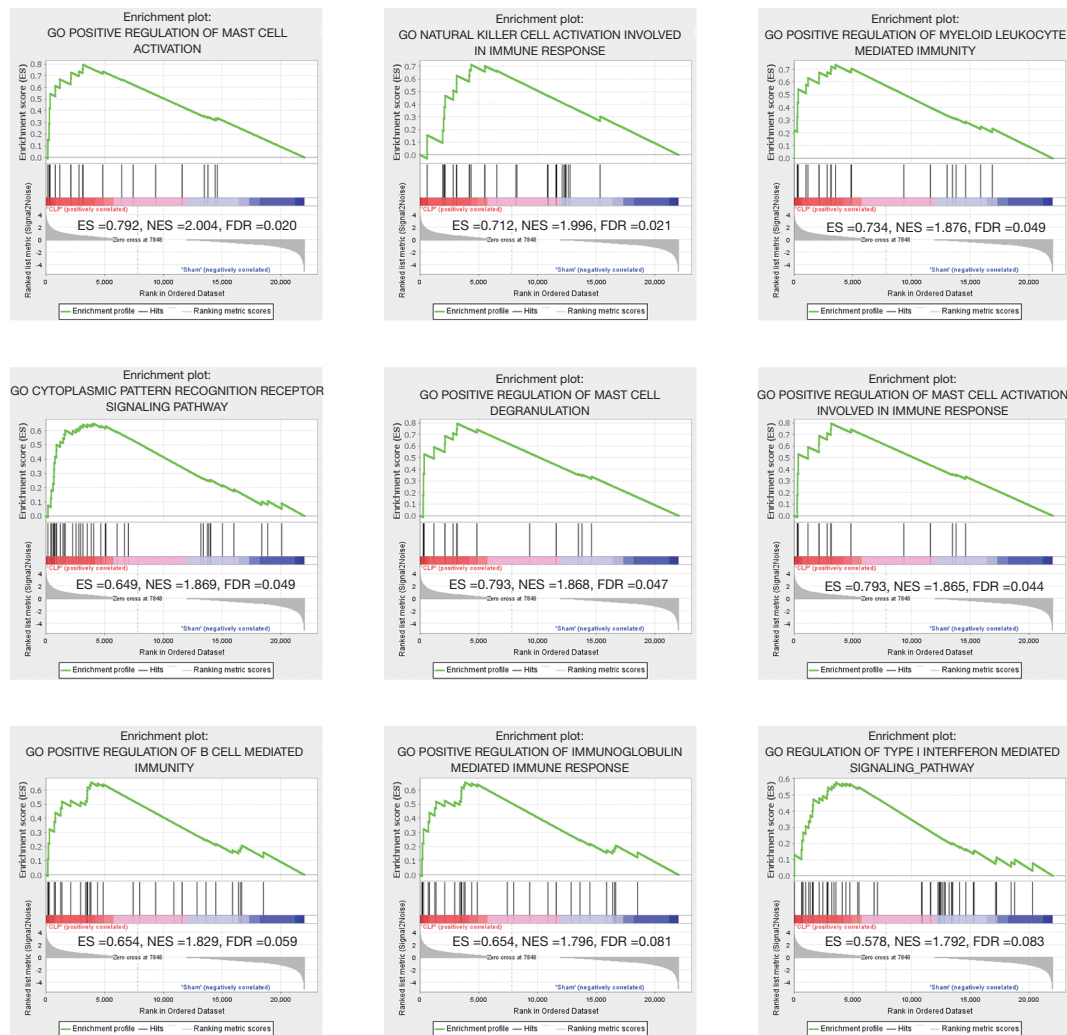


Figure 2 GSEA plot showing the top 9 enriched immune-related gene sets in the CLP and sham groups based on the NES. ES, enrichment score; NES, normalized enrichment score; GSEA, gene set enrichment analysis; FDR, false discovery rate; CLP, cecal ligation and puncture.

kidney RNA samples [CLP group (n=3), sham group (n=2)] were successfully sequenced. We identified a total of 4,754 DEGs in the CLP samples, including 2,322 upregulated genes and 2,432 downregulated genes. Heatmap and volcano plot analyses were used to visualize these DEGs, which are shown in *Figure 1B,1C*.

The DEGs were subjected to GO and KEGG pathway enrichment analyses, and C5 gene sets were used for GSEA to analyze the gene expression profile at an overall level. As shown in *Figure 1D*, GO enrichment analysis of DEGs revealed that the immune response in CLP samples was stronger than the sham samples. For example, biological processes were significantly enriched in neutrophil

aggregation and T-helper 1-cell activation. For the molecular function enrichment, we noted that ferrous iron transmembrane transporter activity was enriched. As shown in *Figure 1E*, KEGG pathway enrichment analysis revealed that DEGs were enriched in ferroptosis (the highest enrichment score), the IL-17 signaling pathway, apoptosis, the PI3K-Akt signaling pathway, and the NF-kappa B signaling pathway. The GSEA results showed that 189 gene sets were significant at a false discovery rate (FDR) <25%, and most of the enriched gene sets were related to various immune responses. *Figure 2* shows the 9 most enriched immune-related gene sets based on the normalized enrichment score (NES). In summary, GSEA revealed

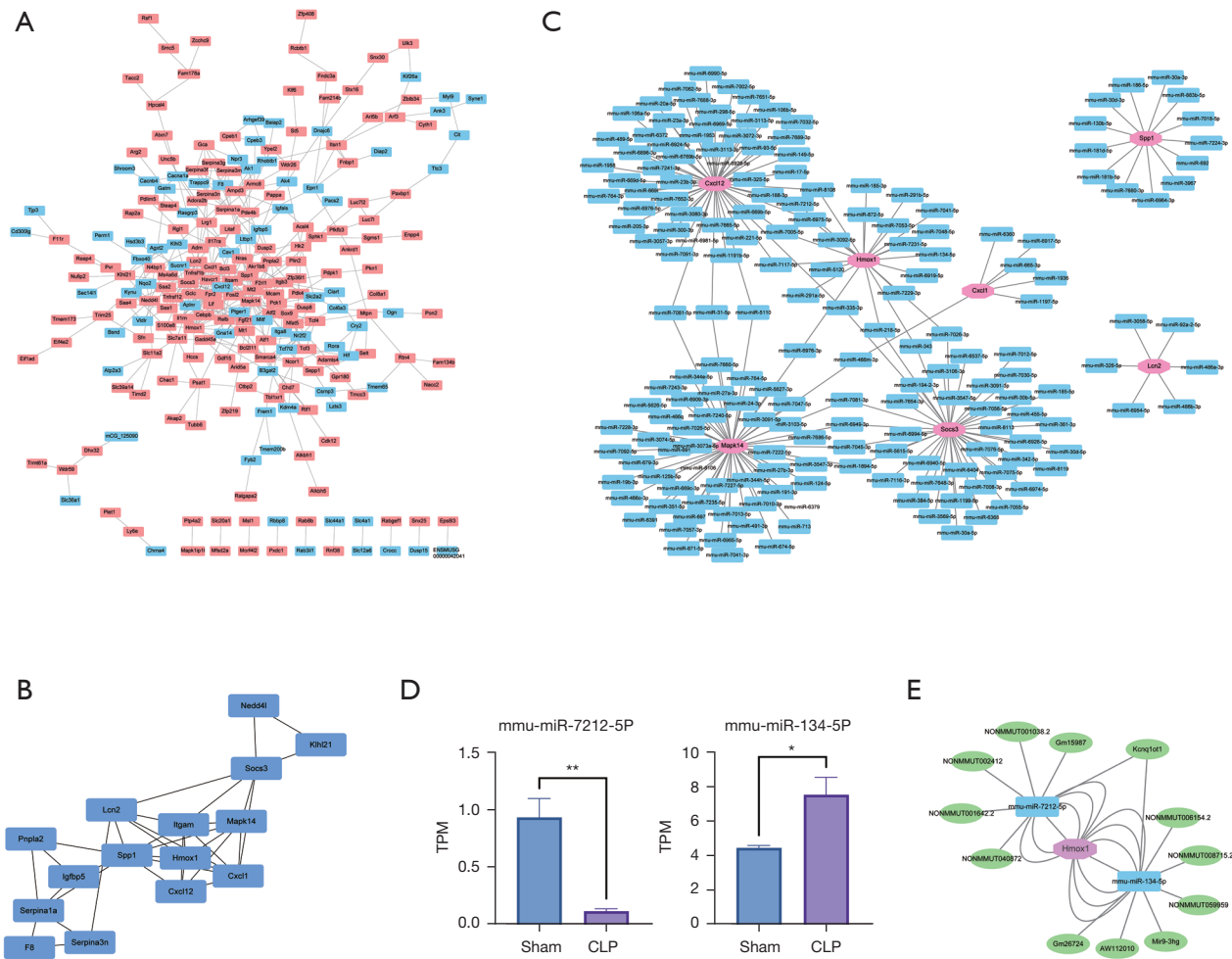


Figure 3 Correlations among DEGs and co-expression networks. (A) The PPI network of DEGs. Each node represents one protein, and each edge represents one protein-protein association. The red nodes represent upregulated genes, and the blue nodes represent downregulated genes. (B) Fifteen hub genes identified by the plugin of MCODE and CytoHubba from the DEGs. (C) A co-expression network of mRNAs and target miRNAs. mRNAs (red nodes) was restricted to the 7 hub genes involved in the KEGG pathway, and miRNAs (blue nodes) were the predicted targets of 7 mRNAs based on the online databases. (D) Expression level of transcripts per million (TPM) between the CLP and sham groups. Left: mmi-miR-7212-5p; right: mmi-miR-134-5p. *P<0.05; **P<0.01. (E) A ceRNA network of Hmox1. The red nodes represent the hub gene Hmox1, the blue nodes represent differentially expressed miRNAs, and the green nodes represent target lncRNAs. DEGs, differentially expressed genes; PPI, protein-protein interaction; MCODE, minimal Common Oncology Data Elements; KEGG, Kyoto Encyclopedia of Genes and Genomes; ceRNA, competitive endogenous RNA; CLP, cecal ligation and puncture.

that the enriched gene sets were related to the activation or regulation of immune cells, the cytoplasmic patterning recognition receptor signaling pathway, and the type I interferon signaling pathway, such as the gene sets of the positive regulation of mast cell activation, natural killer cell activation involved in the immune response, and the positive regulation of myeloid leukocyte-mediated immunity.

PPI network analysis for identifying hub genes and the prediction of target miRNAs for constructing the co-expression network

As shown in *Figure 3A*, the PPI network based on DEGs consisted of 242 nodes and 413 edges. The MCODE plugin was used to identify gene cluster modules, and

Table 2 Fifteen hub genes

Gene symbol	Description	log ₂ FC	Adjusted P value	Regulation
<i>Hmox1</i>	Heme oxygenase 1	4.761	2.753e-05	Up
<i>Cxcl1</i>	Chemokine (C-X-C motif) ligand 1	5.616	3.556e-04	Up
<i>Cxcl12</i>	Chemokine (C-X-C motif) ligand 12	-3.238	5.987e-08	Down
<i>Igfbp5</i>	Insulin-like growth factor binding protein 5	-3.481	2.121e-03	Down
<i>Itgam</i>	Integrin alpha M	4.758	5.308e-05	Up
<i>Klhl21</i>	Kelch-like 21	4.311	1.141e-10	Up
<i>F8</i>	Coagulation factor VIII	-3.626	7.876e-07	Down
<i>Lcn2</i>	Lipocalin 2	6.298	1.599e-10	Up
<i>Mapk14</i>	Mitogen-activated protein kinase 14	4.988	1.030e-06	Up
<i>Nedd4l</i>	Neural precursor cell expressed, developmentally down-regulated gene 4-like	3.150	5.767e-07	Up
<i>Pnpla2</i>	Patatin-like phospholipase domain containing 2	4.134	4.713e-04	Up
<i>Serpina1a</i>	Serine (or cysteine) peptidase inhibitor	7.563	3.742e-25	Up
<i>Serpina3n</i>	Serine (or cysteine) peptidase inhibitor, clade A, member 3N	4.963	9.239e-07	Up
<i>Socs3</i>	Suppressor of cytokine signaling 3	4.914	2.297e-09	Up
<i>Spp1</i>	Secreted phosphoprotein 1	3.503	6.272e-07	Up

FC, fold change.

the results were intersected using cytoHubba (degree and MCC algorithms) to identify hub genes. Fifteen hub genes were identified and are shown in *Figure 3B*. These 15 genes are the key genes in the PPI network and may play important roles in the pathological process of sepsis (*Table 2*). We observed that 7 of the 15 hub genes were involved in the KEGG pathway, including *Hmox1* in ferroptosis, *Lcn2* in the IL-17 signaling pathway, *Cxcl1* and *Cxcl12* in the NF-kappa B signaling pathway, *Mapk14* in the AGE-RAGE signaling pathway in diabetic complications, *Socs3* in the TNF signaling pathway, and *Spp1* in the PI3K-Akt signaling pathway. A total of 183 target miRNAs were predicted based on the 7 hub genes (*Hmox1*, *Spp1*, *Socs3*, *Mapk14*, *Lcn2*, *Cxcl1* and *Cxcl12*), which were involved in the KEGG pathway. Based on the prediction results, a co-expression network of miRNAs and mRNAs was constructed with 190 nodes and 201 edges, as shown in *Figure 3C*.

Because *Hmox1* was the hub gene of ferroptosis, which showed the highest enrichment score from KEGG pathway enrichment analysis, 22 target miRNAs for *Hmox1* were predicted, and the miRNA sequencing results further verified the expression difference between the CLP and sham groups. There were 2 miRNAs, mmu-miR-7212-

5p and mmu-miR-134-5p, which were detected using our miRNA sequencing, and the difference in transcripts per million (TPM) between these 2 groups was statistically significant ($P < 0.05$) (*Figure 3D*).

Thirteen target lncRNAs were predicted based on the differentially expressed miRNAs (mmu-miR-7212-5p and mmu-miR-134-5p) and used to construct ceRNA networks of the *Hmox1* gene (*Figure 3E*).

Verification of the 7 specifically expressed hub genes and the miRNA-*Hmox1* regulatory axis

To verify the expression differences of the predicted 7 hub genes involved in the KEGG pathway, we performed qPCR analysis of mouse kidneys between the CLP and sham groups. We noticed that the mRNA expression levels of the 6 genes (*Hmox1*, *Spp1*, *Socs3*, *Lcn2*, *Cxcl1* and *Cxcl12*) in the 7 expressed hub genes were consistent with the RNA sequencing results (*Figure 4A*).

To further verify the hub gene of *Hmox1* in ferroptosis, we performed Western blotting (*Figure 4B*) to assess the protein expression levels between the CLP and sham groups. Consistent with the qPCR and RNA sequencing

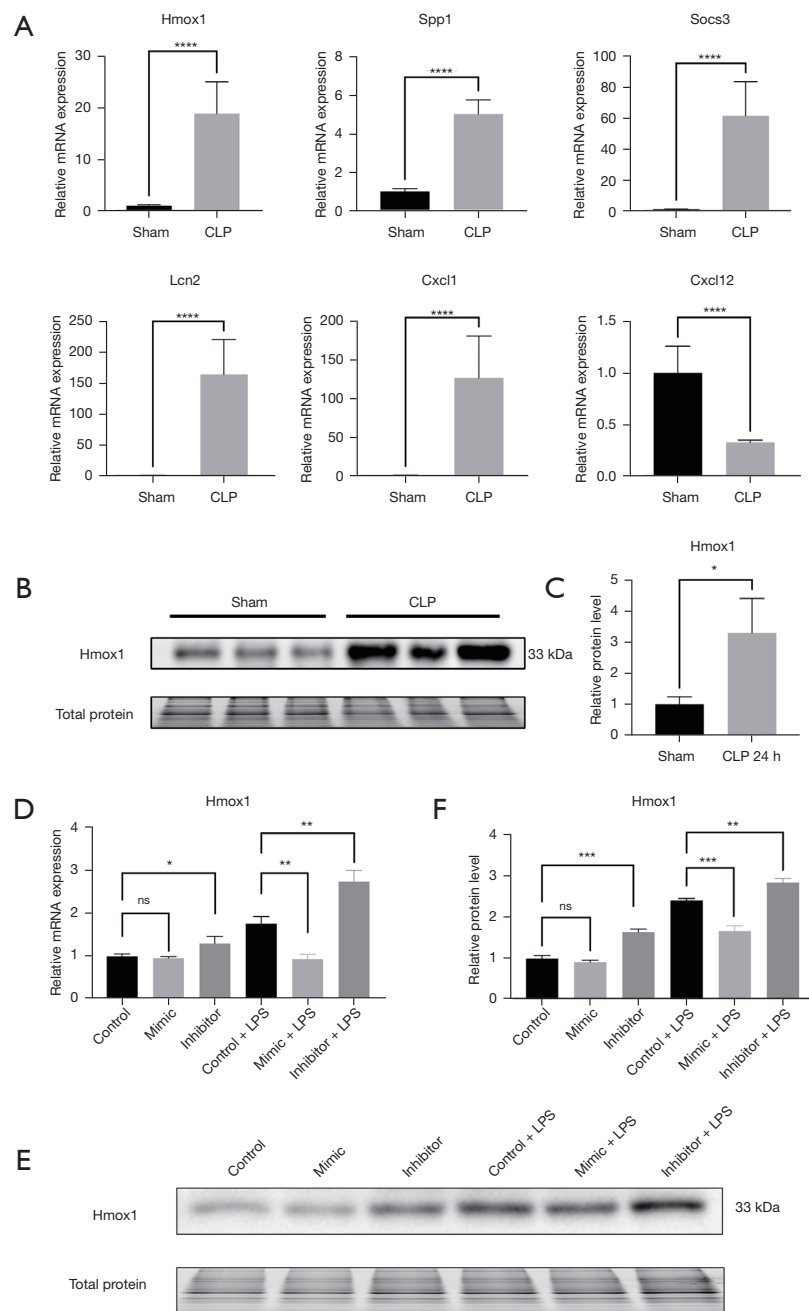


Figure 4 Verification of the predicted hub genes and the miRNA-Hmox1 regulatory axis. (A) qPCR analysis. The mRNA expression levels of 6 hub genes (*Hmox1*, *Spp1*, *Socs3*, *Lcn2*, *Cxcl1* and *Cxcl12*) in mouse kidney tissues (n=3) were consistent with the RNA sequencing results. GAPDH was used as a loading control. (B) Western blotting analysis of Hmox1 in mouse kidney tissues (n=3). Total protein was used as a loading control. (C) Representative densitometric analysis was used to semiquantitatively assess the protein expression levels of Hmox1. (D) qPCR analysis of Hmox1 in TCMK-1 cells treated with an mmu-miR-7212-5p mimic or inhibitor. (E) Western blotting analysis of Hmox1 in TCMK-1 cells treated with an mmu-miR-7212-5p mimic or inhibitor. Total protein was used as a loading control. (F) Representative densitometric analysis was used to semiquantitatively assess the protein expression levels of Hmox1 in the mmu-miR-7212-5p-Hmox1 regulatory axis. *P<0.05; **P<0.01; ***P<0.001; ****P<0.0001. ns, not significant; CLP, cecal ligation and puncture; miRNA, microRNA; qPCR, quantitative real-time polymerase chain reaction; mRNA, messenger RNA; GAPDH, glyceraldehyde 3-phosphate dehydrogenase.

results, the expression of *Hmox1* in CLP kidneys was higher than the sham kidneys (Figure 4C).

The *mmu-miR-7212-5p-Hmox1* regulatory axis was also verified. We noted that in the *mmu-miR-7212-5p-Hmox1* regulatory axis, the mimic of *mmu-miR-7212-5p* reduced the mRNA (Figure 4D) and protein expression (Figure 4E,4F) of *Hmox1* in TCMK-1 cells stimulated with LPS, and its inhibitor increased the mRNA (Figure 4D) and protein expression (Figure 4E,4F) of *Hmox1* in TCMK-1 cells stimulated with or without LPS. These results suggest that *mmu-miR-7212-5p-Hmox1* may be a key RNA regulatory axis that participates in the ferroptosis pathway attributed to the pathophysiological process of SA-AKI.

Inhibitor of mmu-miR-7212-5p attenuates ferroptosis and inflammatory factor release in TCMK-1 cells stimulated with LPS

A previous study demonstrated that *Hmox1* played an anti-ferroptotic role in renal epithelial cells. We wondered whether an inhibitor of *mmu-miR-7212-5p* would attenuate ferroptosis in TCMK-1 cells stimulated with LPS. *Acsl4* is an enzyme that converts fatty acids to fatty acyl-CoA, and it is considered a ferroptosis marker (38). We found that the LPS-induced enhanced mRNA (Figure 5A) and protein expression (Figure 5B,5C) of *Acsl4* in TCMK-1 cells would be attenuated by the *mmu-miR-7212-5p* inhibitor. Flow cytometry results showed that the enhanced ROS level (mean fluorescence intensity of DCFH-DA) in TCMK-1 cells induced by LPS was also attenuated by the *mmu-miR-7212-5p* inhibitor (Figure 5D). MDA is a lipid peroxidation byproduct that reflects the degree of ferroptosis in cells. The MDA content was reduced by the *mmu-miR-7212-5p* inhibitor after LPS challenge (Figure 5E). These data showed that the inhibitor of *mmu-miR-7212-5p* reduced LPS-induced ferroptosis. The *mmu-miR-7212-5p* inhibitor significantly reduced the mRNA expression of *iNOS* and *IL-6*, which indicates that it inhibits the release of LPS-induced renal inflammatory factors (Figure 5F,5G).

m6A RNA Methylation and related regulators involved in SA-AKI

High-throughput sequencing showed that the expression levels of *Alkbh5*, *Igf2bp2* and *Eif3a* were significantly

increased in the CLP groups compared to the controls ($P<0.05$), and the expression levels of *Hnrnpa2b1*, *Igf2bp1*, *Ythdf3*, *Wtap* and *Mettl16* were significantly decreased ($P<0.05$) (Figure 6A). *Wtap* and *Mettl16* are m6A “writers” in the RNA methylation process, *Alkbh5* is an m6A “eraser”, and *Igf2bp1*, *Igf2bp2*, *Eif3a*, *Hnrnpa2b1* and *Ythdf3* are m6A “readers”.

As methyltransferases, *Mettl3* and demethylase *Alkbh5* play core roles in regulating m6A methylation levels. To further investigate whether *Mettl3* and *Alkbh5* were involved in SA-AKI, Western blotting was performed to identify the expression levels of these proteins. As shown in Figure 6B-6E, the results demonstrated that the protein expression of *Mettl3* was decreased in SA-AKI, and the expression of *Alkbh5* was increased. From the data above, we inferred that the total m6A RNA methylation level may be decreased in SA-AKI.

Interaction of m6A RNA methylation-related regulators and CLP hub genes

The interactions of m6A RNA methylation-related regulators were analyzed (Figure 7A), and they were highly connected among writers, erasers and readers. *Mettl3*, *Hnrnpa2b1*, *Hnrnpa2b1* and *Ythdc2* were hub genes in the RNA methylation process because they interacted with at least 18 m6A RNA methylation-related regulators (Figure 7B). The expression levels of *Mettl3*, *Mettl14*, *Mettl16*, *Zc3h13*, *Rbm15b*, *Fto*, *Alkbh5*, *Ythdf1*, *Ythdf2*, *Ythdf3*, *Igf2bp1*, *Igf2bp2* and *Igf2bp3* significantly correlated with the expression levels of other m6A RNA methylation-related regulators ($P<0.05$) (Figure 7C).

To further study the interaction of the m6A RNA methylation-related regulators and 15 hub genes in CLP, we analyzed the correlations between these factors. The correlation analysis of expression revealed that 14 hub genes in CLP were significantly associated with m6A regulators (Figure 7C). The hub gene *Hmox1* positively correlated with the expression of *Ythdf2* and negatively correlated with the expression of *Mettl14*, *Fto*, and *Zc3y13* ($P<0.05$).

The possible m6A modification sites for *Hmox1* were further analyzed. There were at least 21 m6A modification sites, which were supported by at least one m6A-seq or MeRIP-Seq dataset, in the gene sequence of *Hmox1* based on the RMBase database. ‘Motif score’ is an alignment score to evaluate the accuracy of identified motif regions of m6A,

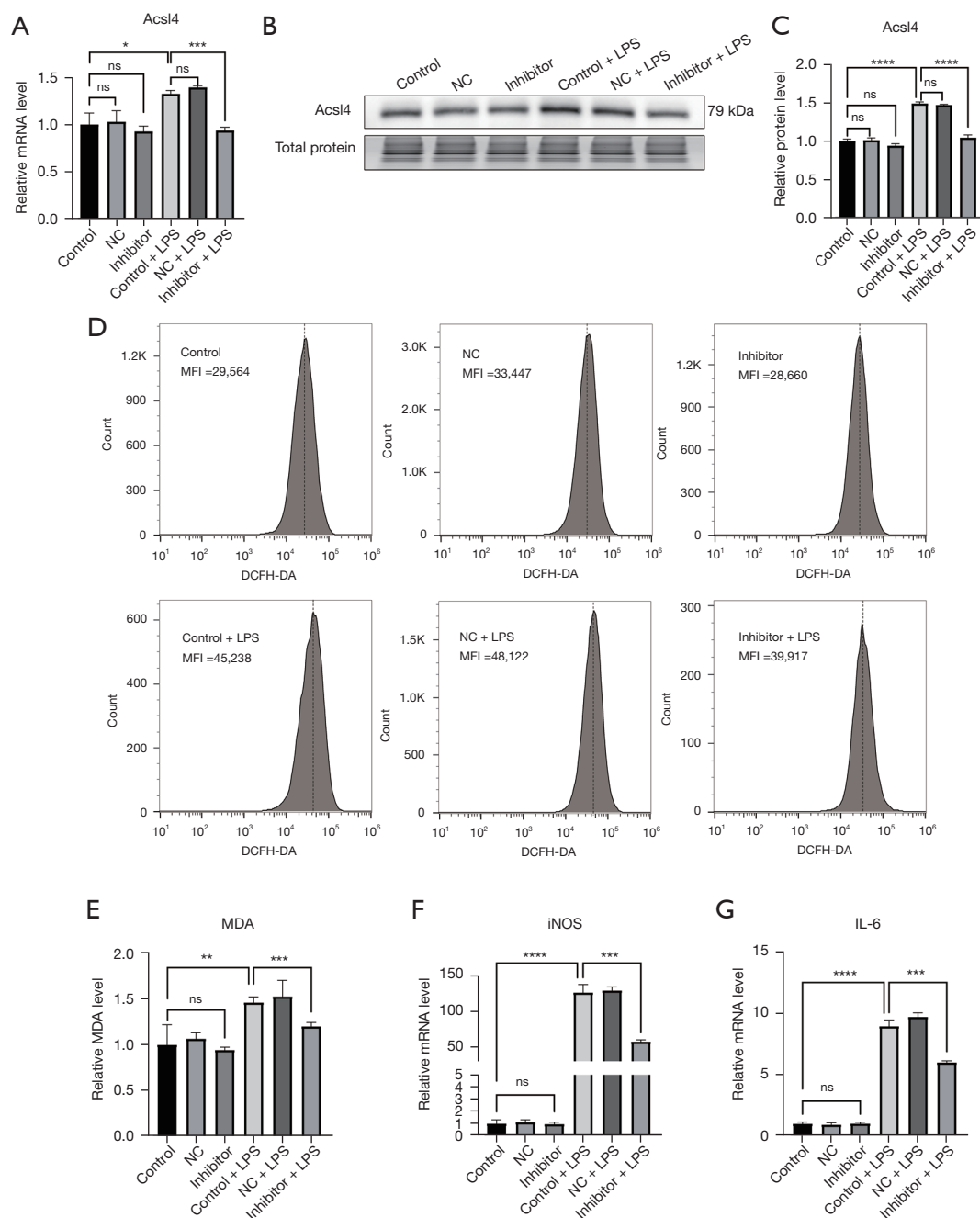


Figure 5 Inhibitor of mmu-miR-7212-5p attenuates ferroptosis and inflammatory factor release in TCMK-1 cells stimulated with LPS. (A) qPCR analysis of *Acsl4* in TCMK-1 cells. (B) Western blotting analysis of *Acsl4* in TCMK-1 cells. Total protein was used as a loading control. (C) Representative densitometric analysis was used to semiquantitatively assess the protein expression levels of *Acsl4*. (D) Flow cytometry analysis of DCFH-DA (2',7'-dichlorodihydrofluorescein diacetate). (E) The intracellular MDA content. (F,G) qPCR analyses of *iNOS* and *IL-6* in TCMK-1 cells. * $P < 0.05$; ** $P < 0.01$; *** $P < 0.001$; **** $P < 0.0001$. ns, not significant; NC, negative control; LPS, lipopolysaccharide; MFI, mean fluorescence intensity; qPCR, quantitative real-time polymerase chain reaction; MDA, malondialdehyde.

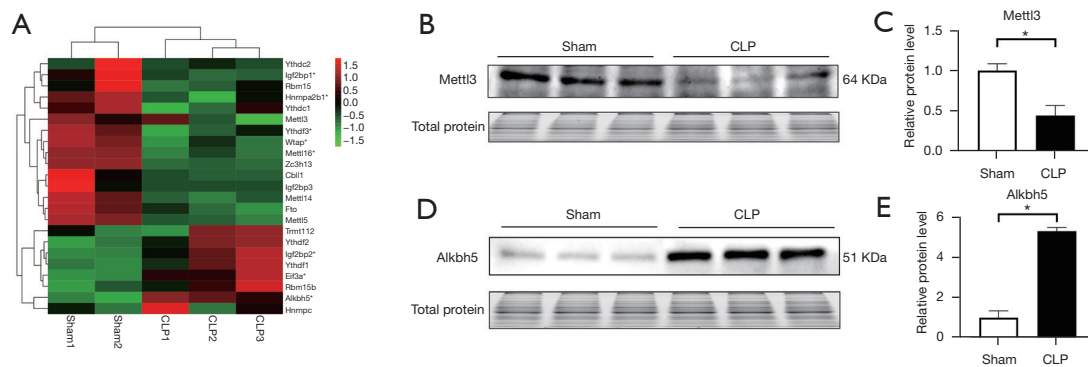


Figure 6 Expression levels of m6A RNA methylation-related regulators. (A) Heatmap of the expression levels of 23 m6A RNA methylation regulators. Asterisks (*) represent significant differences between the two groups ($P < 0.05$). (B-E) Western blotting analysis. Representative densitometric analysis was used to semiquantitatively assess the protein expression levels of the m6A-related enzymes Mettl3 (B,C) and Alkbh5 (D,E) in mouse kidney tissues. Total protein was used as a loading control. Asterisks (*) represent significant differences between the two groups ($P < 0.05$), $n = 3$ per group. m6A, N6-adenosine methylation; CLP, cecal ligation and puncture.

and the sites of the top 10 motif scores are listed in *Table 3*.

Discussion

Sepsis is a highly heterogeneous syndrome that is associated with a dysregulated systemic inflammatory host response to infection and results in organ dysfunction (39). AKI is a major and severe complication in septic patients, but no specific and effective therapeutic strategies are available to treat sepsis-related AKI (40). Therefore, exploring the mechanism of AKI in sepsis is critical for the prevention and treatment of sepsis.

The current study demonstrated that the biological process of GO enrichment analysis showed neutrophil aggregation and T-helper 1-cell activation, and GSEA indicated that most of the enriched gene sets were related to various immune responses, such as the positive regulation of mast cell activation, nature killer cell activation involved in the immune response and the positive regulation of myeloid leukocyte-mediated immunity. These results showed that AKI related to sepsis was accompanied by strong immune activation, which caused inflammation and injury of the renal corpuscle and renal tubule. The current study is the first SA-AKI study to show enriched immune-related pathways using GSEA instead of DEGs. GSEA, which focuses on gene sets, has some advantages compared to single-gene analysis methods (29). GSEA boosts the signal-to-noise ratio, which makes it possible to detect modest

changes in individual genes and effectively reveal important immune-related pathways.

A total of 15 hub genes in the PPI network were obtained by the intersection of two different algorithms, and we noted that 7 (*Hmox1*, *Lcn2*, *Cxcl1*, *Cxcl12*, *Mapk14*, *Socs3* and *Spp1*) of these 15 hub genes were involved in KEGG pathways. The upregulated *Lcn2* in the 7 hub genes was also reported as a hub gene in a previous bioinformatic analysis study of SA-AKI (14), but the other 6 hub genes in the current study had not been reported. To increase the credibility of our bioinformatic analysis, we verified the expression differences of the 7 hub genes *in vivo*. The qPCR results were very consistent with the RNA sequencing results. The upregulated or downregulated expression of the 7 genes played key roles in different signaling pathways. We further constructed a co-expressed network of the 7 mRNAs and their target miRNAs. This network demonstrated the interaction mechanism by which the most key genes were regulated at the transcriptome level.

Our enrichment pathway results were generally consistent with a previous bioinformatics study (15), such as the apoptotic process and the responses to cytokine and immune system process pathways. However, we also noted that the ferroptosis pathway was enriched and had the highest enrichment score. The molecular function of GO enrichment analysis found that ferrous iron transmembrane transporter activity was enriched. Among these 7 hub genes, *Hmox1* in the ferroptosis pathway was in the center

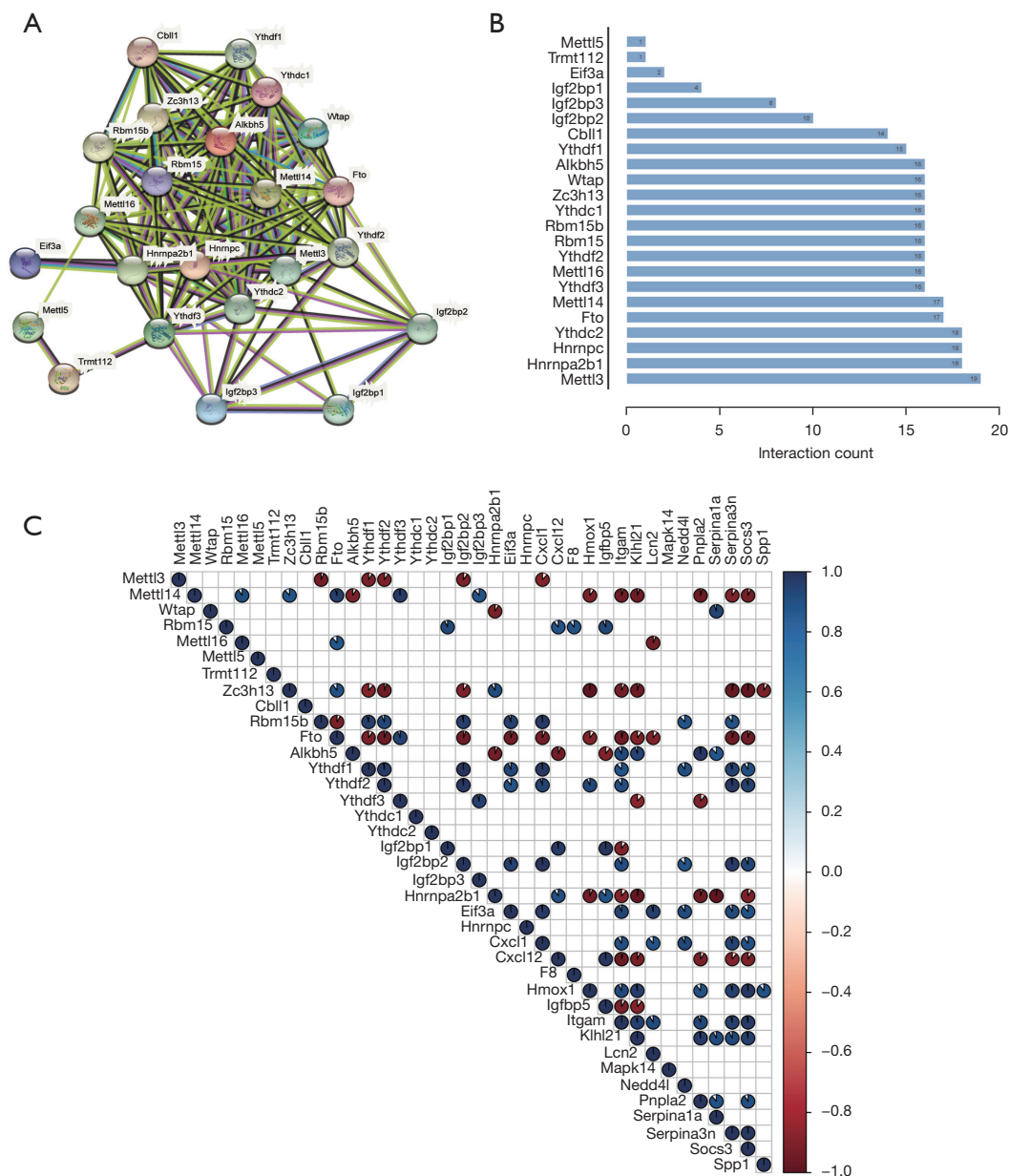


Figure 7 Interactions of m6A RNA methylation-related regulators. (A) The protein-protein interactions among 23 m6A methylation regulators. (B) The rank of connection degrees (interaction counts) of 23 m6A RNA methylation regulators. (C) Spearman correlations between 23 m6A-related enzymes and 15 CLP hub genes. The red pie chart represents a negative correlation between the 2 genes ($P < 0.05$), and the blue pie chart represents a positive correlation between the 2 genes ($P < 0.05$). The area of the pie chart represents the absolute value of the correlation coefficient. m6A, N6-adenosine methylation; CLP, cecal ligation and puncture.

of the hub gene PPI network, with 6 edges connected with other hub genes. The mRNA and protein expression of Hmox1 was upregulated in the kidneys of the CLP group. These results indicate that the ferroptosis pathway plays an important role in the pathophysiological events of the

kidney in sepsis.

Ferroptosis is a novel iron-dependent cell death pathway that is characterized by increases in reactive oxygen species (ROS) and lipid peroxidation caused by iron overloading (41). Ferroptosis is the key mechanism in the pathogenesis of

Table 3 The m6A modifications analysis of Hmox1

Sequence
CTCTCCTTAGCCCAGCTGGGACTTCTTTACTCTCCTCTTTG
AAGGGCTGCCCTGGAGCAGGACATGGCCTTCTGGTATGGGC
ATCGAGCAGAACCAGCCTGA ^{Mod} ACTAGCCCAGTCCGGTGATGG
GAATGCTGAGTTCATGAAGA ^{Mod} CTTTCAGAAGGGTCAGGTGT
CTGGCCCCCAGGGGCTGTGA ^{Mod} ACTCTGTCCAATGTGGCCTTC
ACATCCAGCCAGTGGCCTGA ^{Mod} ACTTTGAAACCAGCAGCCCCA
GGCTTTTTTTACCTTCCCGAACATCGACAGCCCCACCAAGT
GCTCTATCGTGCTCGA ^{Mod} ATGAACACTCTGGAGATGACACCTG
CAGGTGATGCTGACAGAGGAACACAAAGACCAGAGTCCCTC
AAATCAGAAATAGGGTACAGACAAAAGCGCCCAGGGTAAGC

m6A, N6-adenosine methylation; Mod, modification; italic A, m6A modification site.

AKI, and the disruption of iron homeostasis is a significant contributor to tissue injury (42). Deferoxamine (DFO) inhibits lipid peroxidation and renal tubular epithelial cell necrosis to prevent renal failure (43).

Hmox1, namely, heme oxygenase-1 (HO-1), is a phase II enzyme that metabolizes heme into biliverdin/bilirubin and ferrous iron, and it triggers the generation of carbon monoxide and H-ferritin (42,44). To further elucidate the potential mechanism of Hmox1, the present study constructed a ceRNA network of the target lncRNAs and miRNAs for Hmox1. The Hmox1 gene was upregulated in the CLP group, and its target miRNA, mmu-miR-7212-5p, was downregulated in the CLP group. According to the miRNA hypothesis, we hypothesized that mmu-miR-7212-5p-Hmox1 was a key RNA regulatory pathway. To test this hypothesis, we verified the mmu-miR-7212-5p-Hmox1 regulatory axis. LPS stimulation led to a distinct compensatory elevation of Hmox1 expression in TCMK-1-cell lines, and a mmu-miR-7212-5p mimic attenuated LPS-induced enhanced Hmox1 expression but further increased by the inhibitor. However, without LPS stimulation, this phenomenon was only observed in the mmu-miR-7212-5p inhibitor, and the reduction in Hmox1 levels was not significant for the mimic. The reasons for this result may be that without LPS stimulation, the expression of Hmox1 is relatively low, and the expression of mmu-miR-7212-5p is relatively high. The expression level of Hmox1 could not be further decreased by exogenous additional mmu-miR-7212-5p mimic.

Ferroptosis is a pro-inflammatory agent that recruits macrophages and causes inflammation in AKI (45). Recent studies revealed that Hmox1 played an anti-ferroptotic role during AKI against oxidative stress and inflammation (43). By upregulating the Hmox1 pathway, LPS-induced acute lung injury was reduced, and lung pathological changes were ameliorated (46). We found that an inhibitor of mmu-miR-7212-5p increased the expression of Hmox1 and attenuated ferroptosis by reducing the expression of Acl4. Acl4 is a known promoter of ferroptosis that regulates lipid biosynthesis by converting fatty acids to fatty acyl-CoA esters. Ablation of the Acl4 gene attenuates the pathological and functional injury of AKI mice (38). ROS formation is considered the executioner of ferroptosis. Excessive ROS cause oxidative stress and exacerbate mitochondrial dysfunction, which lead to renal injury directly (47). The increased ROS level activates the inflammatory response to remote organ injury (48). The LPS-induced ROS levels and inflammatory factor release in TCMK-1 cells were reduced as a result of attenuated ferroptosis. Taken together, our study indicates that the mmu-miR-7212-5p-Hmox1 axis participates in the pathophysiological process of sepsis-induced AKI induced. The inhibitor of mmu-miR-7212-5p may be a potential clinical therapeutic target for sepsis-related AKI.

m6A is one of the most ubiquitous and abundant mRNA methylation modifications that occur in eukaryotes (49), and it is closely related to the heterogeneity and prognosis of sepsis (50). There were 21 m6A modification sites in the sequence of the hub gene Hmox1, which indicated that Hmox1 may be modified by m6A RNA methylation. Meanwhile, it has been reported that mmu-miR-7212-5p in the predicted regulatory pathway may also be regulated by Mettl3-mediated m6A modifications (51). These results suggested that SA-AKI may be regulated by m6A methylation.

To further verify this assumption, we first identified 8 differentially expressed m6A RNA methylation-related regulators. As shown in the heatmap in *Figure 6A*, in addition to the 8 significantly differentially expressed m6A genes, the overall gene expression levels of 23 m6A RNA methylation-related regulators were obviously different between the CLP and control groups. The Western blotting results showed that the protein expression of Mettl3 (a core writer) was decreased in SA-AKI, and the expression of Alkbh5 (a core eraser) was increased. Notably, the mRNA expression levels of *Mettl3* between sham and CLP in the heatmap were not significant due to the

individual differences of mice. The *Mettl3* protein levels are more persuasive because of the methyltransferase function in the form of protein. These results suggested that RNA methylation modification played an important role in the pathophysiological process of AKI induced by sepsis, and the total abundance of m6A may be downregulated.

The PPI network and expression correlation analyses showed close interactions among m6A RNA methylation regulators. We noted that *Hmox1*, with 21 m6A modification sites, showed numerous correlations with m6A methylation regulators, such as *Mettl14* and *Hnrnpa2b1*. These results indicated that m6A “writers”, “erasers” and “readers” may interact with hub genes and play a synergistic role in RNA methylation modifications to influence the expression of hub genes, especially *Hmox1*. To the best of our knowledge, the present study is the first transcriptome-wide study to propose the possible involvement of m6A RNA methylation in the pathophysiological process of AKI induced by sepsis and provide a possible mechanism.

The primary goal of this study was to provide as many novel directions as possible using bioinformatics analyses for further mechanistic research and potential clinical therapeutic strategies for SA-AKI. The association between m6A RNA methylation modifications and SA-AKI was exported in silicon. However, the limitations of this study were that the roles of m6A RNA methylation-related regulators in AKI induced by sepsis were primarily deduced from high-throughput sequencing analysis. Although we performed qPCR and Western blotting experiments *in vivo* and *in vitro* to verify the bioinformatic analysis results, the mechanisms underlying m6A RNA methylation regulation and the verification of signaling pathways must be demonstrated in further experiments, such as MeRIP-Seq. The sample size was relatively limited. Therefore, future studies should increase the sample size.

Conclusions

The present study identified 7 key genes (*Hmox1*, *Spp1*, *Socs3*, *Mapk14*, *Lcn2*, *Cxcl1* and *Cxcl12*) that were significantly involved in signaling pathways. We found that mmu-miR-7212-5p-*Hmox1* in ferroptosis was a key RNA regulatory pathway that participated in the pathophysiological process of SA-AKI. Our study demonstrated the expression profiles and potential functions of m6A RNA methylation regulators in SA-AKI, which significantly correlated with some hub genes and promoted the progression of AKI.

Acknowledgments

Funding: This work was supported by the Fund of the Improvement of Scientific and Technological Innovation Ability Project of Army Medical University (No. 2019XQY18 to Xia Yang) and the Fund of the National Natural Science Foundation of China (Nos. 82070072 and 81873644 to Xinjin Chi).

Footnote

Reporting Checklist: The authors have completed the ARRIVE reporting checklist. Available at <https://atm.amegroups.com/article/view/10.21037/atm-22-845/rc>

Data Sharing Statement: Available at <https://atm.amegroups.com/article/view/10.21037/atm-22-845/dss>

Conflicts of Interest: All authors have completed the ICMJE uniform disclosure form (available at <https://atm.amegroups.com/article/view/10.21037/atm-22-845/coif>). The authors have no conflicts of interest to declare.

Ethical Statement: The authors are accountable for all aspects of the work in ensuring that questions related to the accuracy or integrity of any part of the work are appropriately investigated and resolved. Experiments were performed under a project license (No. AMUWEC20201509) granted by the Laboratory Animal Welfare and Ethics Committee of Third Military Medical University, in compliance with the Third Military Medical University institutional guidelines for the care and use of animals.

Open Access Statement: This is an Open Access article distributed in accordance with the Creative Commons Attribution-NonCommercial-NoDerivs 4.0 International License (CC BY-NC-ND 4.0), which permits the non-commercial replication and distribution of the article with the strict proviso that no changes or edits are made and the original work is properly cited (including links to both the formal publication through the relevant DOI and the license). See: <https://creativecommons.org/licenses/by-nc-nd/4.0/>.

References

1. Singer M, Deutschman CS, Seymour CW, et al. The Third International Consensus Definitions for Sepsis and Septic Shock (Sepsis-3). *JAMA* 2016;315:801-10.

2. Poston JT, Koyner JL. Sepsis associated acute kidney injury. *BMJ* 2019;364:k4891.
3. Dou Q, Tong H, Yang Y, et al. PICK1 Deficiency Exacerbates Sepsis-Associated Acute Kidney Injury. *Biomed Res Int* 2021;2021:9884297.
4. Peerapornratana S, Manrique-Caballero CL, Gómez H, et al. Acute kidney injury from sepsis: current concepts, epidemiology, pathophysiology, prevention and treatment. *Kidney Int* 2019;96:1083-99.
5. Yoshimoto K, Komaru Y, Iwagami M, et al. Acute Kidney Injury in Sepsis: Evidence From Asia. *Semin Nephrol* 2020;40:489-97.
6. Kellum JA, Romagnani P, Ashuntantang G, et al. Acute kidney injury. *Nat Rev Dis Primers* 2021;7:52.
7. Scholz H, Boivin FJ, Schmidt-Ott KM, et al. Kidney physiology and susceptibility to acute kidney injury: implications for renoprotection. *Nat Rev Nephrol* 2021;17:335-49.
8. Yong WP, Rha SY, Tan IB, et al. Real-Time Tumor Gene Expression Profiling to Direct Gastric Cancer Chemotherapy: Proof-of-Concept “3G” Trial. *Clin Cancer Res* 2018;24:5272-81.
9. Almansa R, Ortega A, Ávila-Alonso A, et al. Quantification of Immune Dysregulation by Next-generation Polymerase Chain Reaction to Improve Sepsis Diagnosis in Surgical Patients. *Ann Surg* 2019;269:545-53.
10. Wu K, Nie B, Li L, et al. Bioinformatics analysis of high frequency mutations in myelodysplastic syndrome-related patients. *Ann Transl Med* 2021;9:1491.
11. Zhang Q, Hu H, Chen SY, et al. Transcriptome and Regulatory Network Analyses of CD19-CAR-T Immunotherapy for B-ALL. *Genomics Proteomics Bioinformatics* 2019;17:190-200.
12. Wu J, Qin Y, Li Z, et al. Comprehensive analysis of lncRNA and miRNA expression profiles and ceRNA network construction in negative pressure wound therapy. *Ann Transl Med* 2021;9:1383.
13. Cheng Q, Chen X, Wu H, et al. Three hematologic/immune system-specific expressed genes are considered as the potential biomarkers for the diagnosis of early rheumatoid arthritis through bioinformatics analysis. *J Transl Med* 2021;19:18.
14. Tang Y, Yang X, Shu H, et al. Bioinformatic analysis identifies potential biomarkers and therapeutic targets of septic-shock-associated acute kidney injury. *Hereditas* 2021;158:13.
15. Yang JJ, Wu BB, Han F, et al. Gene expression profiling of sepsis-associated acute kidney injury. *Exp Ther Med* 2020;20:34.
16. Wei CM, Gershowitz A, Moss B. Methylated nucleotides block 5' terminus of HeLa cell messenger RNA. *Cell* 1975;4:379-86.
17. Du J, Liao W, Liu W, et al. N6-Adenosine Methylation of Socs1 mRNA Is Required to Sustain the Negative Feedback Control of Macrophage Activation. *Dev Cell* 2020;55:737-753.e7.
18. Huang H, Weng H, Chen J. m6A Modification in Coding and Non-coding RNAs: Roles and Therapeutic Implications in Cancer. *Cancer Cell* 2020;37:270-88.
19. Tong J, Flavell RA, Li HB. RNA m6A modification and its function in diseases. *Front Med* 2018;12:481-9.
20. Zhao BS, Roundtree IA, He C. Post-transcriptional gene regulation by mRNA modifications. *Nat Rev Mol Cell Biol* 2017;18:31-42.
21. Qu F, Tsegay PS, Liu Y. N6-Methyladenosine, DNA Repair, and Genome Stability. *Front Mol Biosci* 2021;8:645823.
22. Sun T, Wu R, Ming L. The role of m6A RNA methylation in cancer. *Biomed Pharmacother* 2019;112:108613.
23. Qin Y, Li L, Luo E, et al. Role of m6A RNA methylation in cardiovascular disease (Review). *Int J Mol Med* 2020;46:1958-72.
24. Fan H, Le JW, Sun M, et al. Sirtuin 3 deficiency promotes acute kidney injury induced by sepsis via mitochondrial dysfunction and apoptosis. *Iran J Basic Med Sci* 2021;24:675-81.
25. Li Y, Zhai P, Zheng Y, et al. Csf2 Attenuated Sepsis-Induced Acute Kidney Injury by Promoting Alternative Macrophage Transition. *Front Immunol* 2020;11:1415.
26. Chen S, Zhou Y, Chen Y, et al. fastp: an ultra-fast all-in-one FASTQ preprocessor. *Bioinformatics* 2018;34:i884-90.
27. Langmead B, Salzberg SL. Fast gapped-read alignment with Bowtie 2. *Nat Methods* 2012;9:357-9.
28. Wickham H. *ggplot2: Elegant Graphics for Data Analysis*. 2nd ed. Use R! Cham: Springer International Publishing; Imprint: Springer, 2016. doi:10.1007/978-3-319-24277-4.
29. Subramanian A, Tamayo P, Mootha VK, et al. Gene set enrichment analysis: a knowledge-based approach for interpreting genome-wide expression profiles. *Proc Natl Acad Sci U S A* 2005;102:15545-50.
30. Szklarczyk D, Gable AL, Lyon D, et al. STRING v11: protein-protein association networks with increased coverage, supporting functional discovery in genome-wide experimental datasets. *Nucleic Acids Res* 2019;47:D607-13.
31. Agarwal V, Bell GW, Nam JW, et al. Predicting effective

- microRNA target sites in mammalian mRNAs. *Elife* 2015;4:e05005.
32. Sticht C, De La Torre C, Parveen A, et al. miRWalk: An online resource for prediction of microRNA binding sites. *PLoS One* 2018;13:e0206239.
 33. Chen Y, Wang X. miRDB: an online database for prediction of functional microRNA targets. *Nucleic Acids Res* 2020;48:D127-31.
 34. Gong J, Liu C, Liu W, et al. LNCediting: a database for functional effects of RNA editing in lncRNAs. *Nucleic Acids Res* 2017;45:D79-84.
 35. Yang C, Hu Y, Zhou B, et al. The role of m6A modification in physiology and disease. *Cell Death Dis* 2020;11:960.
 36. Li Y, Ge YZ, Xu L, et al. The Potential Roles of RNA N6-Methyladenosine in Urological Tumors. *Front Cell Dev Biol* 2020;8:579919.
 37. Xuan JJ, Sun WJ, Lin PH, et al. RMBase v2.0: deciphering the map of RNA modifications from epitranscriptome sequencing data. *Nucleic Acids Res* 2018;46:D327-34.
 38. Wang Y, Zhang M, Bi R, et al. ACSL4 deficiency confers protection against ferroptosis-mediated acute kidney injury. *Redox Biol* 2022;51:102262.
 39. Vandewalle J, Libert C. Sepsis: a failing starvation response. *Trends Endocrinol Metab* 2022;33:292-304.
 40. Guo C, Ye FX, Jian YH, et al. MicroRNA-214-5p aggravates sepsis-related acute kidney injury in mice. *Drug Dev Res* 2022;83:339-50.
 41. Lei P, Bai T, Sun Y. Mechanisms of Ferroptosis and Relations With Regulated Cell Death: A Review. *Front Physiol* 2019;10:139.
 42. Scindia Y, Leeds J, Swaminathan S. Iron Homeostasis in Healthy Kidney and its Role in Acute Kidney Injury. *Semin Nephrol* 2019;39:76-84.
 43. Adedoyin O, Boddu R, Traylor A, et al. Heme oxygenase-1 mitigates ferroptosis in renal proximal tubule cells. *Am J Physiol Renal Physiol* 2018;314:F702-14.
 44. Chiang SK, Chen SE, Chang LC. A Dual Role of Heme Oxygenase-1 in Cancer Cells. *Int J Mol Sci* 2018;20:39.
 45. Wang Y, Quan F, Cao Q, et al. Quercetin alleviates acute kidney injury by inhibiting ferroptosis. *J Adv Res* 2021;28:231-43.
 46. Li J, Lu K, Sun F, et al. Panaxydol attenuates ferroptosis against LPS-induced acute lung injury in mice by Keap1-Nrf2/HO-1 pathway. *J Transl Med* 2021;19:96.
 47. Ueda N. A Rheostat of Ceramide and Sphingosine-1-Phosphate as a Determinant of Oxidative Stress-Mediated Kidney Injury. *Int J Mol Sci* 2022;23:4010.
 48. Li JY, Yao YM, Tian YP. Ferroptosis: A Trigger of Proinflammatory State Progression to Immunogenicity in Necroinflammatory Disease. *Front Immunol* 2021;12:701163.
 49. Gu J, Zhan Y, Zhuo L, et al. Biological functions of m6A methyltransferases. *Cell Biosci* 2021;11:15.
 50. Zhang S, Liu F, Wu Z, et al. Contribution of m6A subtype classification on heterogeneity of sepsis. *Ann Transl Med* 2020;8:306.
 51. Mi B, Xiong Y, Yan C, et al. Methyltransferase-like 3-mediated N6-methyladenosine modification of miR-7212-5p drives osteoblast differentiation and fracture healing. *J Cell Mol Med* 2020;24:6385-96.

Cite this article as: Liu B, Ao S, Tan F, Ma W, Liu H, Liang H, Yang X, Chi X. Transcriptomic analysis and laboratory experiments reveal potential critical genes and regulatory mechanisms in sepsis-associated acute kidney injury. *Ann Transl Med* 2022;10(13):737. doi: 10.21037/atm-22-845